

Neuromorphic Quantum Neural Networks with Tunnel-Diode Activation Functions

Jake McNaughton, A. H. Abbas*, and Ivan S. Maksymov
Artificial Intelligence and Cyber Futures Institute,
Charles Sturt University, Bathurst, NSW 2795, Australia
Email: aborae@csu.edu.au

Abstract—The mathematical complexity and high dimensionality of neural networks hinder the training and deployment of machine learning (ML) systems while also requiring substantial computational resources. This fundamental limitation drives ML research, particularly in the exploration of alternative neural network architectures that integrate novel building blocks, such as advanced activation functions. Tunnel diodes are well-known electronic components that utilise the physical effect of quantum tunnelling (QT). Here, we propose using the current-voltage characteristic of a tunnel diode as a novel, physics-based activation function for neural networks. We demonstrate that the tunnel-diode activation function (TDAF) outperforms traditional activation functions in terms of accuracy and loss during both training and evaluation. We also highlight its potential for implementation in electronic circuits suited to developing neuromorphic, quantum-inspired AI systems capable of operating in environments not suitable for qubit-based quantum computing hardware.

I. INTRODUCTION

THE fields of machine learning (ML) and neuromorphic computing (NC) are rapidly evolving, with increasing demands for energy-efficient and biologically plausible computational models [1], [2]. Algorithmic neural network models rely on activation functions [3]—mathematical functions applied to the output of a neuron—that enable deep learning architectures to learn complex patterns in the input data [4]. The nonlinearity of activation functions is crucial for modelling intricate relationships between inputs and outputs, enabling the neural network to generalise beyond the training data [3]–[5]. Without nonlinearity, neural networks reduce to linear models, limiting their ability to capture and learn hierarchical representations found in real-world data [3]. However, commonly used activation functions such as ReLU, sigmoid and tanh exhibit limitations, particularly in deep learning, due to issues such as vanishing gradients and energy inefficiency [4]. These challenges hinder learning in deep networks, necessitating alternative solutions that offer both efficient computation and reduced power consumption [4], [6], [7].

Physics, particularly quantum mechanics, has profoundly influenced ML, inspiring the development of novel algorithms that exploit physical principles to enhance computational efficiency and reduce power consumption [1], [2], [8], [9]. A notable example is quantum reservoir computing (RC) [10]–[12], a subclass of neuromorphic and unconventional computing systems [13] that employs the intrinsic dynamics of physical systems to enable energy-efficient ML solutions, particularly for predicting highly nonlinear and chaotic time

series, as well as for pattern recognition tasks [11], [12]. Concurrently, physics-informed neural networks integrate fundamental physical laws—expressed through partial differential equations—directly into the learning process [14]. This approach ensures that models remain consistent with established physical principles while requiring fewer data points compared to traditional deep learning methods.

Quantum neural networks (QNNs) are computational models that integrate quantum mechanics with traditional neural network architectures used in ML [15], [16]. Modern research on QNNs focuses on integrating classical artificial neural networks—widely used in ML and computer vision [4]—with the unique advantages of quantum information processing [17], [18].

QNNs and NC systems share the goal of replicating cognitive processes observed in biological brains [8], [9], [19]–[22]. Both QNNs and NC systems aim to overcome the limitations of conventional computing, which relies on deterministic logic and sequential processing. NC systems address these challenges through event-driven architectures and parallel processing, mimicking the function of biological neurons and synapses [19]–[21].

Quantum tunnelling (QT) has been utilised in tunnel [23] and resonant-tunnelling diodes [24], with certain NC architectures exploiting negative differential resistance [22], [25], a hallmark of tunnelling diodes. QT-based devices, including tunnel diodes, exhibit significantly lower power consumption than traditional integrated circuits [26], also exhibiting a number of characteristics essential for applications in challenging environments such as space [27]. Additionally, QT has facilitated the development of scanning tunnelling microscopy (STM) [28] and has also been experimentally observed in quantum dots [25], which serve as essential components of quantum NC systems [10].

Recent advancements in quantum computing have increasingly employed QT in quantum annealing and NC systems [29]. In quantum annealing, tunnelling enables systems to traverse potential energy barriers, aiding the discovery of optimal solutions in combinatorial optimisation problems [29]. In other classes of NC systems, QT mechanisms have been integrated to emulate the architecture of the brain [30]. Finally, QT also plays a critical role in quantum biology, influencing enzymatic reactions and energy transfer in photosynthesis [31].

The mathematical expressions governing the probability of QT through a potential barrier exhibit rich nonlinear properties [32] and semiconductor diodes serve as a key element of NC

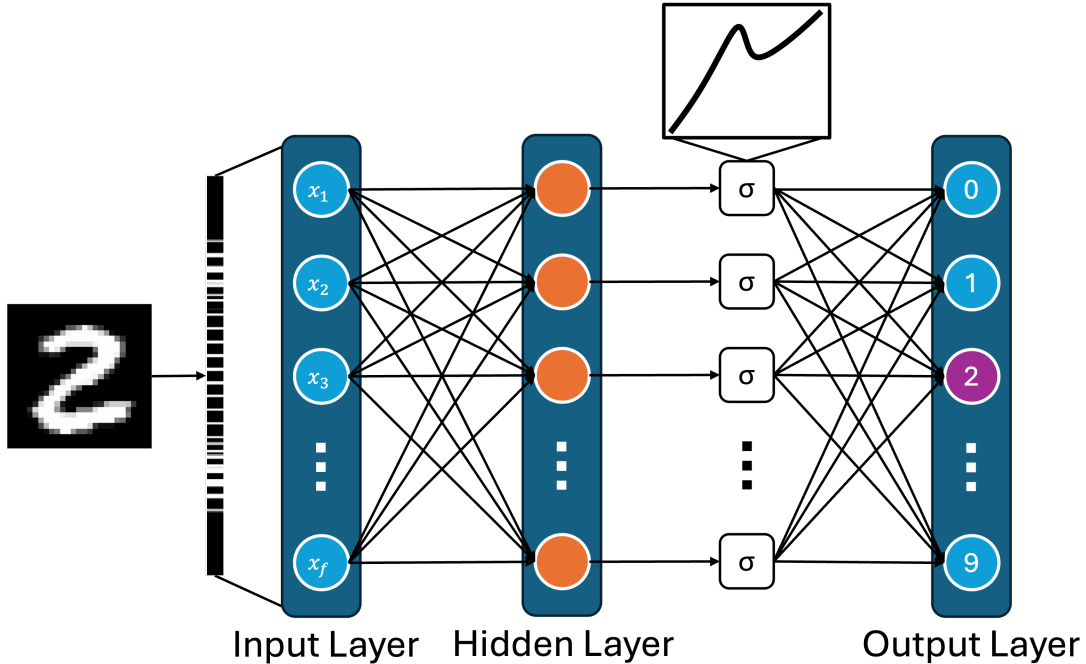


Fig. 1. Architecture of a neural network using the current–voltage characteristic of a tunnel diode (inset) as a nonlinear activation function, referred to as TDAF in the main text.

systems [33]. Therefore, in this paper we propose and theoretically demonstrate that the current–voltage (I–V) characteristic of a tunnel diode can serve as a novel nonlinear activation function in neural networks (Fig. 1). Unlike conventional activation functions, which are often heuristic and lack direct physical interpretations, the intrinsic nonlinearity of the tunnel diode arises from well-defined quantum mechanical principles [34], [35]. By systematically comparing traditional activation functions used in ML, we show that the neural network implementing the tunnel-diode activation function (TDAF) not only exhibits superior performance in terms of convergence, accuracy and expressiveness of the model but also introduces an energy-efficient approach to neuromorphic computing by extending prior research work [32]. This quantum-inspired activation function opens new possibilities for designing more biologically plausible and computationally efficient neural architectures, further bridging the gap between semiconductor physics and quantum AI systems.

II. METHODS

A. Traditional Activation Functions

The nonlinearity of activation functions enables neural networks to model complex patterns beyond what linear transformations alone can achieve [4]. Various activation functions have been developed, each with advantages and limitations [4], [7].

For example, sigmoid $f(x) = \frac{1}{1 + e^{-x}}$ and hyperbolic tangent (tanh) $f(x) = \frac{e^x - e^{-x}}{e^x + e^{-x}}$ functions [4], [19], [36] compress inputs into a fixed range $(0, 1)$ and $(-1, 1)$, respectively. However, while useful for probability estimation and feature

scaling, these functions suffer from saturation, where large or small inputs lead to near-zero gradients, hindering weight updates in multilayer networks [4].

Therefore, one of the most widely used activation functions is the Rectified Linear Unit (ReLU), defined as $f(x) = \max(0, x)$ [4]. ReLU is computationally efficient and helps mitigate some of the vanishing gradient problems associated with sigmoid and tanh functions. However, ReLU is not fully immune to gradient-related issues, since neurons based on this function can become inactive when they consistently receive negative inputs, which prevents further learning [4]. To address this limitation, variants such as Leaky ReLU and Parametric ReLU have been proposed, which introduce small negative slopes for negative inputs to maintain gradient flow and prevent inactive neurons [6]. Other functions such as Swish $f(x) = x \cdot \sigma(x)$, where $\sigma(x)$ is the sigmoid function, and GELU have been introduced to balance smoothness and gradient propagation [7]. Commonly used in transformer models, these activation functions offer improved expressiveness but remain not universally optimal [7].

Thus, no single activation function is ideal for all tasks, as each has trade-offs in efficiency, stability and expressiveness [7]. The quest for a universal nonlinear function remains open, with researchers exploring biologically inspired models, adaptive activation mechanisms and quantum-inspired functions that could enhance learning dynamics across diverse architectures and applications [10], [32].

B. Tunnel-Diode Activation Function

A tunnel diode exploits the effects of QT, enabling charge carriers to pass through an energy barrier rather than overcoming it thermally [23]. Unlike conventional p-n junctions,

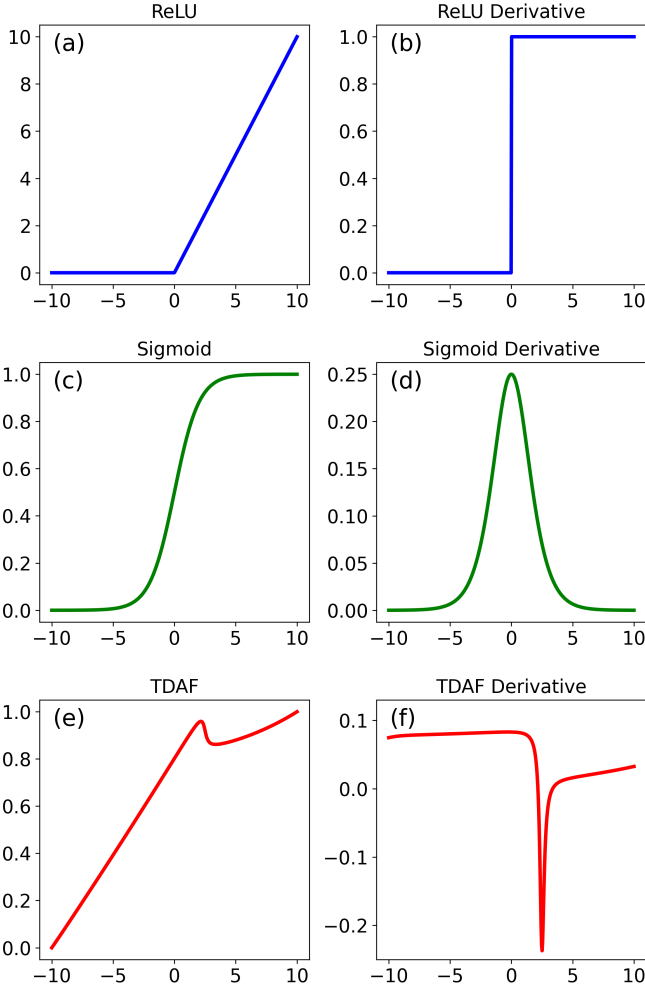


Fig. 2. Two commonly used activation functions (ReLU and sigmoid) and their derivatives, alongside the proposed activation function, TDAF.

tunnel diodes are heavily doped, reducing the depletion width to just a few nanometres [35]. This extreme doping causes the conduction band of the n-region and the valence band of the p-region to become energetically aligned, enabling electrons to tunnel directly through the barrier.

At zero bias and small forward bias, electrons tunnel from the conduction band of the n-region to the valence band of the p-region, resulting in a sharp increase in current. As voltage increases further, band misalignment reduces the probability of QT, causing a drop in current—a phenomenon known as negative differential resistance. At even higher voltages, QT ceases entirely and the diode behaves like a standard p-n junction. This transport mechanism enables tunnel diodes to operate at high speeds and low power levels, making them valuable for high-frequency and microwave applications.

Mathematically, the current-voltage (I–V) characteristic curve of a tunnel diode is a highly nonlinear function, primarily due to a negative differential resistance region, and it is given by

$$I(V) = J_1(V) + J_2(V), \quad (1)$$

where

$$J_1(V) = a \ln \left(\frac{1 + e^{\alpha + \eta V}}{1 + e^{\alpha - \eta V}} \right) \times \left(\frac{\pi}{2} + \tan^{-1} \left(\frac{c - n_1 V}{d} \right) \right)$$

and $J_2(V) = h (e^{\gamma V} - 1)$.

The parameters are defined as $\alpha = \frac{q(b-c)}{k_B T}$, $\eta = \frac{q n_1}{k_B T}$ and $\gamma = \frac{q n_2}{k_B T}$, where q is the electron charge, k_B is Boltzmann's constant, T is the temperature, V is the voltage, and a , b , c , d , n_1 and n_2 are parameters characterising the physical system. In this work, we use $T = 300$ K, $a = 0.0039$ A, $b = 0.5$ V, $c = 0.0874$ V, $d = 0.0073$ V, $n_1 = 0.0352$, $n_2 = 0.0031$ and $h = 0.0367$ A, with all as per Ref. [37] except b , which has been scaled by a factor of 10 to explore the nonlinear behaviour of TDAF.

From both a physics and mathematics perspective, TDAF, as defined by Eq. (1), can be separated into three distinct regions [37]: two regions of positive differential resistance separated by a central region of negative differential resistance (approximately in the x -axis range from 1 to 3 in Fig. 2e). The first term of Eq. (1), $J_1(V)$, dominates at lower voltages, producing the positive differential resistance region at low voltage and the negative differential resistance region, but fails to capture the region of increasing current after the tunnelling region. The second term, $J_2(V)$, dominates at higher voltages and produces the second positive differential resistance region [38].

When compared to ReLU and sigmoid (Fig. 2a, c), TDAF, from an ML perspective, exhibits two main regions: a nominally weakly nonlinear region for negative inputs which corresponds to the first positive differential resistance region of the I–V characteristic, and a nominally highly nonlinear region for positive inputs which corresponds to the negative differential resistance region and the second positive differential resistance region of the I–V characteristic. Upon comparing the derivative plots of ReLU and TDAF (Fig. 2b, f), it is reasonable to expect that these two functions will exhibit similar ML behaviour. Additionally, we argue that TDAF exhibits a greater degree of nonlinearity compared to ReLU and sigmoid activation functions, as demonstrated below.

C. Analysis of Nonlinear Properties of TDAF

Analysing the degree of nonlinearity is a non-trivial task, as no standard metrics exist, and nonlinearity itself arises from diverse physical and mathematical processes. For example, one method to compare the nonlinearity of activation functions is to analyse their Taylor series expansions and compare the magnitudes of the higher-order terms. However, the Taylor series is an approximation and calculating its coefficients can be non-trivial, especially for artificial functions such as ReLU.

Consequently, a previous study [39] suggested that two nonlinear physical phenomena can be compared by examining the Fourier spectra of a linear signal processed by the nonlinear systems of interest. Following this approach, we analyse the responses of the ReLU, sigmoid and TDAF activation functions to a purely sinusoidal wave signal at a frequency of 16 Hz. For the sake of comparison, we also apply the

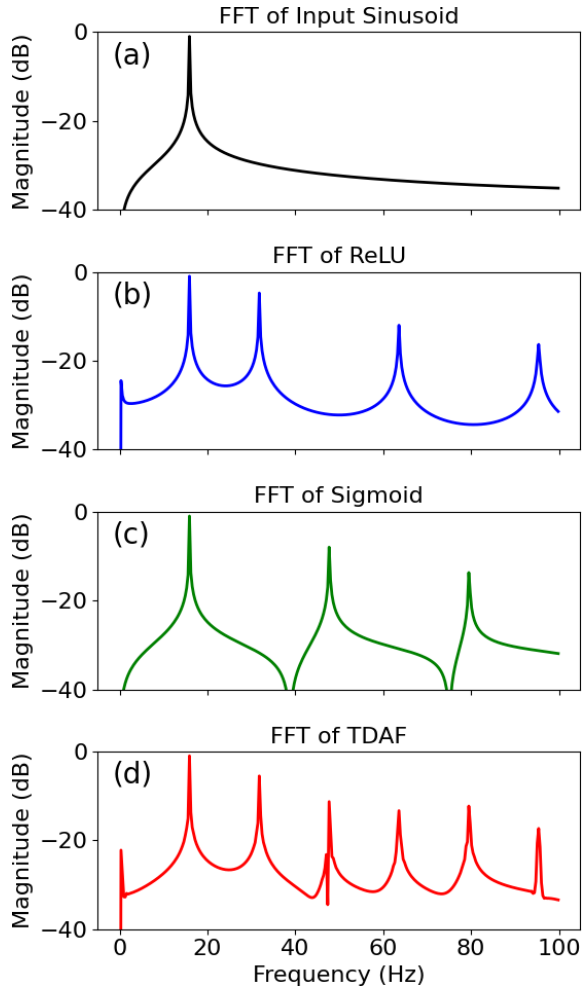


Fig. 3. Fourier spectra of the outputs of (b) ReLU, (c) sigmoid and (d) TDAF functions activated by a sinusoidal wave signal at a frequency of 16Hz. Panel (a) shows the spectrum of the reference output produced by the linear identity function.

sinusoidal signal to a linear identity function, producing a Fourier spectrum with a sole peak at 16 Hz.

As shown in Fig. 3, the response of ReLU, sigmoid and TDAF to the sinusoidal waves results in the nonlinear generation of higher-order harmonics. According to [39], the strength of the nonlinearity can be quantified using the magnitude of the harmonic peaks and the total number of harmonics produced by the nonlinear process. Focusing on the latter criterion, we can see that ReLU produces the peak at the second-harmonic frequency 32 Hz and then at the fourth, 64 Hz, and the sixth, 96 Hz, harmonics. In turn, sigmoid produces the third, 48 Hz, and fifth, 80 Hz, peaks only. On the contrary, TDAF generates strong peaks at both odd and even harmonic frequencies. Within the theoretical framework used in this analysis [39], this result suggests that the TDAF exhibits the strongest nonlinearity among the three analysed functions. We also observe that both TDAF and ReLU exhibit DC components in their respective spectra, which further supports our earlier assumption of their similar responses.

The selection of a simple sinusoidal input signal for analysing the spectra of the activation functions carries sig-

nificant meaning from an ML and NC perspective. It was demonstrated that a traditional RC algorithm, which can, in principle, employ any standard neural activation function [19], is mathematically equivalent to a model that uses both linear weights of an input dataset and its nonlinear (quadratic, cubic and so on) functionals [40]. It follows from Ref. [40] that the computational efficiency of the model can be increased by constructing an algorithm or using a suitable, either theoretical or real-life physical, dynamical system that is highly nonlinear enough to expand the input data over many higher-order nonlinear functionals. This assertion was confirmed experimentally using a fluid-mechanical dynamical system employed as a neuromorphic computer [41]. In light of this discussion, TDAF outperforms both ReLU and sigmoid, as its Fourier spectrum contains all nonlinear harmonics, with their respective magnitudes being stronger, thus enabling better generation of nonlinear functionals of the input data and resulting in higher computational efficiency.

D. Neural Networks

Feedforward neural networks (FNNs)—the foundational model considered in this paper—typically consist of an input layer, L hidden layers and an output layer [42]. The l th hidden layer, containing N_l neurons, takes an input vector, $x^{(l-1)}$, from the previous layer and applies a linear transformation

$$F : x^{(l-1)} \rightarrow W^{(l)}x^{(l-1)} + b^{(l)}, \quad (2)$$

where $W^{(l)} \in M^{N_{l-1} \times N_l}$ and $b^{(l)} \in \mathbb{R}^{N_l}$ are the weight matrix and bias vector of layer l that are applied to input data received from layer $l-1$. An activation function, $\sigma^{(l)}$ is then applied to the output to obtain the input to the next layer $x^{(l)} = \sigma^{(l)}(a^{(l)})$, where $a^{(l)} = F(x^{(l-1)})$ [43], [44]. The neural network \mathcal{N} is then the composition of the functions comprising these layers (see Fig. 1 for an illustration)

$$\mathcal{N} := F_{L+1} \circ \sigma_L \circ F_L \circ \cdots \circ \sigma_1 \circ F_1, \quad (3)$$

where F_{L+1} is the linear transformation performed by the output layer. The input layer does not perform any computations.

Thus, nonlinearity is introduced into the neural network through the activation functions $\sigma_1, \dots, \sigma_{L+1}$, which, in the framework of an individual model, are typically all the same function, $\sigma_i = \sigma : \mathbb{R} \rightarrow \mathcal{R}$, $\forall i$ [3]–[5]. FNNs employing nonlinear activation functions have been shown to be universal function approximators [45]. For many common activation functions, the range, \mathcal{R} , is $[0, 1]$ or $[-1, 1]$.

Importantly, provided the domains encompass \mathbb{R} , an activation function σ can be replaced with another function σ' , such as TDAF (see the inset in Fig. 1), without changing other aspects of the structure of the neural network. However, the optimal ranges for the hyperparameters, including learning rate, batch size and number of epochs, may differ between two distinct activation functions [46].

In supervised classification problems, the network is responsible for determining the class to which a given sample from the dataset belongs [4]. The dataset consists of samples belonging to C different classes. Each sample is a pair (x_i, y_i) , where x_i is the input data and y_i is the one-hot encoding of

the class that the data belongs to (a vector of length C with a 1 at the index corresponding to the class and zeros elsewhere). The output layer of the neural network produces a vector \hat{y} of length C and the index of the maximum value in the output vector corresponds to the predicted class.

In order for the network to improve on its predictions, a loss function \mathcal{L} is required to quantify the performance. In classification tasks, cross-entropy is commonly used as the loss function [4]

$$\mathcal{L} = - \sum_{c=1}^C y_c \log \left(\frac{e^{\hat{y}_c}}{\sum_{i=1}^C e^{\hat{y}_i}} \right), \quad (4)$$

where the argument of the logarithm can be interpreted as the predicted probability of sample belonging to class c [47], calculated from the output vector \hat{y} as

$$\hat{p}_c = \frac{e^{\hat{y}_c}}{\sum_{i=1}^C e^{\hat{y}_i}}. \quad (5)$$

Optimising the loss function takes place through applying a gradient descent algorithm to the parameters $W^{(l)}$ and $b^{(l)}$ across all layers [4].

To optimise \mathcal{L} with respect to the weights $W^{(l)}$ and biases $b^{(l)}$, gradient backpropagation is employed [4]. This involves computing the gradients of the loss function with respect to the network parameters. Using the chain rule, the gradient $\frac{\partial \mathcal{L}}{\partial W^{(l)}}$ is calculated as

$$\frac{\partial \mathcal{L}}{\partial W^{(l)}} = \delta^{(l)} \cdot (x^{(l-1)})^T, \quad (6)$$

where $\delta^{(l)}$ represents the error at layer l , propagated backward through the network

$$\delta^{(l)} = \left((W^{(l+1)})^T \delta^{(l+1)} \right) \odot \sigma'(a^{(l)}), \quad (7)$$

where $(W^{(l+1)})^T$ is the transpose of the weight matrix from layer l to $l+1$, \odot is the element-wise multiplication operator

and $\sigma'(a^{(l)})$ is the derivative of the activation function at $a^{(l)}$. Then, the error at the output layer is computed as

$$\delta^{(L)} = \hat{y} - y. \quad (8)$$

Using these gradients, the parameters are updated via gradient descent

$$W^{(l)} \leftarrow W^{(l)} - \eta \frac{\partial \mathcal{L}}{\partial W^{(l)}}, \quad (9)$$

$$b^{(l)} \leftarrow b^{(l)} - \eta \frac{\partial \mathcal{L}}{\partial b^{(l)}}, \quad (10)$$

where η is the learning rate parameter.

E. Numerical Experiments and Datasets

Figure 1 illustrates the general feed-forward neural network architecture used in this paper, with the inset specifically showing how TDAF is incorporated into the model. Each network consists of three layers: an input layer, a single hidden layer and an output layer. Three topologically identical neural networks were implemented in PyTorch, with the only distinction being the activation function applied after the hidden layer: ReLU, sigmoid or TDAF.

The standard MNIST handwritten digits dataset [48] was used to benchmark the model. MNIST consists of 70,000 28×28 images that are split into predefined training and test sets of 60,000 and 10,000 images, respectively. Consequently, the input layer received a 28×28 image flattened into a one-dimensional vector of length 784. The flattened and normalised data served as the input into the first hidden layer, which was a fully connected layer consisting of 128 neurons. The output then passed through an activation function (ReLU, sigmoid or TDAF), before being sent through the output layer which consisted of 10 neurons, producing logits for classification.

Additionally, to prevent extreme numerical values from entering Eq. (1), the input was clamped between -10 and 10 (the choice of clamping limits depends on the specific data and task). The output was normalised between 0 and 1. The corresponding source code is available at [49].

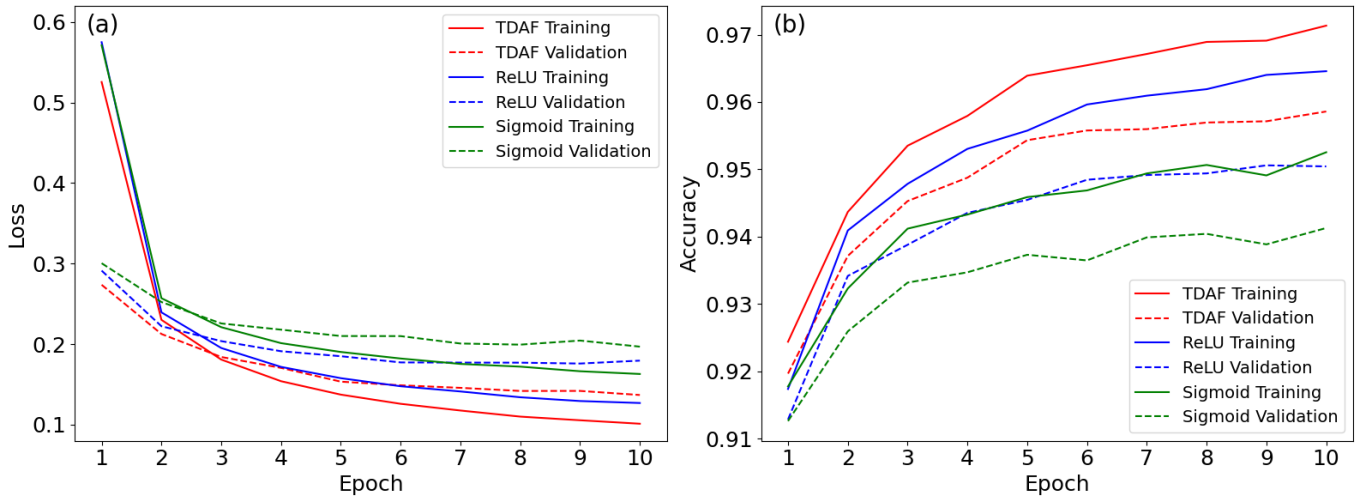


Fig. 4. (a) Loss curves obtained for the neural networks using ReLU, sigmoid and TDAF. (b) Accuracy curves obtained for the neural networks using ReLU, sigmoid and TDAF. The initial accuracy values before the first epoch are not shown – all were around 10%.

III. RESULTS

The neural network architecture shown in Fig. 1 was trained through 10 epochs with a learning rate of 0.01 and a batch size of 256. The MNIST training data was randomly split into 80% training and 20% validation, and the accuracy and loss values after each epoch were recorded for the training and validation sets. This training procedure was applied to the three topologically identical networks that utilised ReLU, sigmoid and TDAF, respectively. To account for variations caused by the random initialisation, the entire experiment was repeated 20 times. For each activation function, the means of the losses and accuracies after each epoch across the 20 repeats was recorded. All computations were performed on an Apple Macbook Pro M3 using an 8-core CPU.

A. Loss and Accuracy Throughout Training

Figure 4a shows the learning curves of the training and validation sets for the three different activation functions. We demonstrate that the network with the TDAF activation function achieves a lower loss at every epoch for both the training and validation sets. The loss of the TDAF network on the training set reached 0.1012 compared to 0.1269 for ReLU and 0.1630 for sigmoid. On the validation set, TDAF reached a loss of 0.1369, whereas ReLU reached 0.1796 and sigmoid reached 0.1969. Figure 4b shows the accuracy throughout training for both the training and validation sets. In this context, the TDAF network also shows superior performance across both the training and validation sets for all epochs.

B. Accuracy on Test Dataset

Each model was trained 20 times to reduce statistical noise caused by the initialisation and to measure the deviations between different runs. Figure 5 demonstrates the performance of the models on the test set after training, showing the median and interquartile range. TDAF achieves a mean accuracy of 96.14% on the test set, compared to 95.32% for ReLU and 94.44% for sigmoid. This result is similar to the final accuracies of the validation set of 95.86%, 95.04% and 94.13% for TDAF, ReLU and sigmoid, respectively. Thus, outperforming the other activation functions based on the median and mean test accuracy, TDAF also exhibits a smaller interquartile range and overall range indicating more stable training dynamics. Additionally, TDAF outperforms both Sigmoid and ReLU in terms of the loss and accuracy throughout training as well as the performance on the test set after training.

Since TDAF has demonstrated superior characteristics compared to other activation functions, we assess the performance of the TDAF-based neural network across the ten classes of the MNIST dataset. Figure 6 presents the loss during training, the confusion matrix and the accuracy across different classes. The class accuracies range from 92.73% for the digit 2 to 98.07% for the digit 4. The most frequent misclassification was for the digits 2 being identified as a digit 8, occurring 42 times—an outcome that aligns with empirical observations [50]. It is noteworthy that the strong performance observed in this study, despite the simplicity of the FNN model, underscores

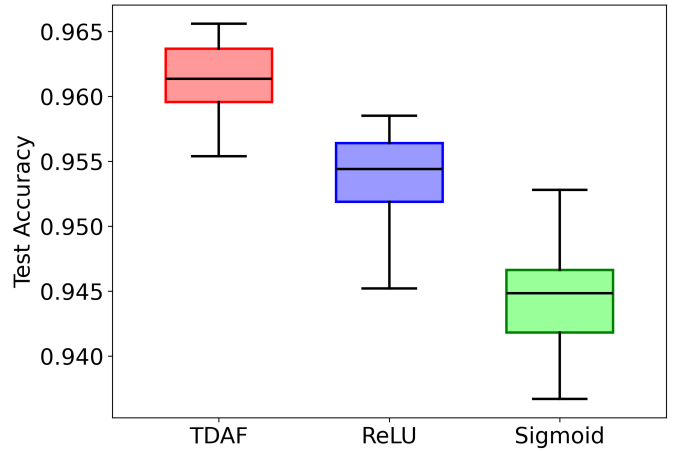


Fig. 5. Box and whisker plot showing the median accuracy and interquartile range (IQR). The coloured boxes denote the value of IQR, with the straight line inside each box corresponding to the respective median value. The top and bottom straight lines located outside each box denote the high and low outliers, respectively.

the advantages conferred by TDAF, demonstrating its potential to enhance classification accuracy in neural networks with minimal architectural complexity.

IV. DISCUSSION

The successful adaption of the characteristic I-V curve of a tunnel diode as an activation function for neural networks raises interesting questions on the underlying mechanisms causing the improved performance and potential future applications. TDAF exhibited superior training dynamics, stability and accuracy on the MNIST dataset compared with the sigmoid and ReLU activation functions. This suggests that the TDAF creates a simpler loss landscape when compared to ReLU and sigmoid.

The mechanism behind the superior performance of TDAF can potentially be explained by exploring the physical phenomena present in tunnel diodes—in particular, the effect of QT. The physically nonlinear (non-monotonic) nature of the TDAF, created by two positive differential resistance regions separated by a region of negative differential resistance, allows for efficient exploration of the local loss landscape, which may contribute to increased stability in training whilst exploring a broader area of the local optimisation landscape.

In practice, a TDAF-based neural network can be implemented using readily available commercial tunnelling [23] and resonant tunnelling [24] diodes. It is noteworthy that systems based on tunnelling diodes consume significantly less power than traditional integrated electronic circuits [26], presenting an opportunity for developing semiconductor chips optimised for power-constrained applications, such as autonomous vehicles, where onboard energy resources are highly limited [9]. Furthermore, NC schemes that exploit negative differential resistance—a key characteristic of tunnelling diodes—have already been proposed [22], [25], suggesting that TDAF functionality could be integrated into existing systems.

Alternatively, a TDAF can be implemented using scanning tunnelling microscopy (STM) instrumentation [28]. STM

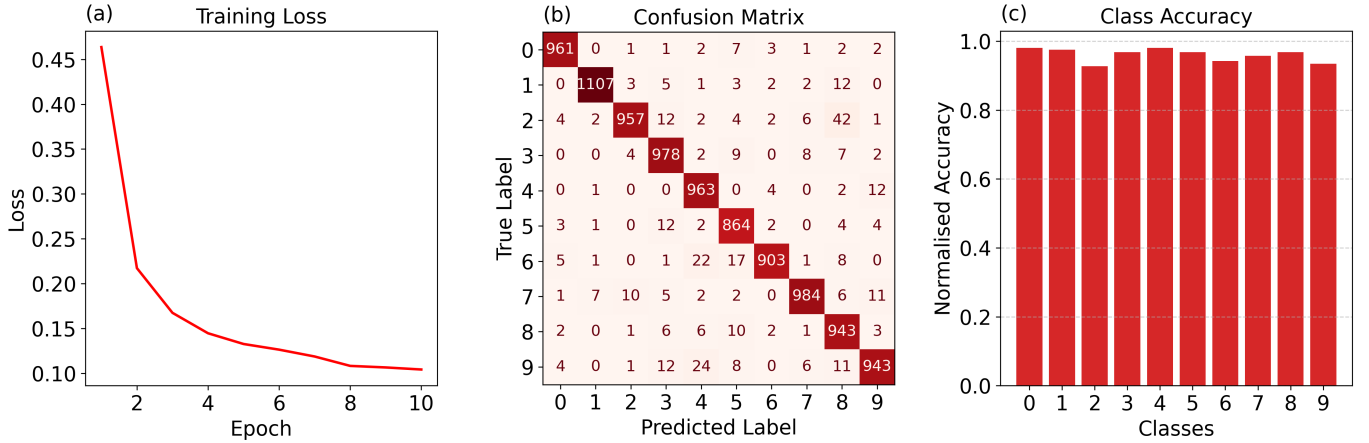


Fig. 6. Results from the TDAF neural network evaluated on the test set. (a) shows the loss throughout training, (b) shows the confusion matrix comparing the predicted labels to the true labels for each class, and (c) summarises the performance on each class.

amplifiers operate at microwave frequencies, providing high signal-to-noise ratios and enabling differential resistance spectroscopy measurements [51], which can be used to compute the derivative of TDAF. In low-frequency designs, this derivative can also be obtained using simple analog electronic circuits [52]. Furthermore, QT of individual electrons has been experimentally observed in quantum dots [25], which serve as fundamental building blocks for quantum NC systems and can therefore be integrated with them [10].

AI will be pivotal in future space exploration, but significant technological challenges must be addressed, particularly in energy consumption and thermal management [53]. Modern AI systems rely on efficient cooling to dissipate heat from graphics processing units, yet the vacuum of space renders conventional air-based cooling methods ineffective [53]. This makes heat dissipation a critical concern for spacecraft, satellites and space exploration vehicles, necessitating innovative cooling solutions to ensure the reliable operation of sensitive electronics in extreme environments [54].

Tunnel diodes, known for their high-speed operation, low noise and resilience in extreme conditions, are widely used in space applications such as high-frequency oscillators, amplifiers and satellite transceivers [27]. Their high radiation hardness, particularly in materials like gallium arsenide (GaAs) or indium phosphide (InP), ensures reliability in space missions, while their exceptional performance at cryogenic temperatures makes them valuable for astrophysics instruments [27]. This highlights the potential of TDAF as a transformative solution to replace the expensive, high-power-consuming and less reliable electronic systems currently used in ground-based AI.

V. CONCLUSION

We introduced a novel activation function, the tunnel-diode activation function (TDAF), derived from the current–voltage (I–V) characteristic of a tunnel diode. TDAF demonstrated superior performance compared to two widely used activation functions—ReLU and sigmoid—achieving higher accuracy and lower loss during both training and evaluation. Furthermore, TDAF exhibited stable behaviour throughout training,

highlighting its robustness across different machine learning tasks.

We suggested that the improved performance of TDAF can be attributed to the QT effect that underpins the operation of tunnel diodes. This effect introduces greater nonlinearity and expands data into a broader set of nonlinear functionals, enabling ML algorithms to process information more efficiently. This physically grounded approach opens new avenues for integrating quantum-inspired mechanisms into ML models, bridging the gap between AI and emerging neuromorphic computing paradigms.

Future research will focus on further theoretical exploration of the QT-based nonlinearity of TDAF and its implications for network dynamics. Additionally, practical implementation of TDAF in hardware-based neuromorphic circuits will be pursued, potentially enabling the development of energy-efficient, high-speed AI systems capable of operating in environments unsuitable for conventional or qubit-based quantum computing hardware.

Comparing the performance of TDAF implementations across different neural network architectures—such as recurrent and convolutional neural networks, RC systems and transformer-based models—will further test the robustness of the activation function and establish which types of tasks TDAF performs best. Moreover, studying how activation functions affect the loss landscape will provide insight into whether other physically inspired functions may offer advantages for ML applications.

As previously mentioned, our results indicate that implementing tunnel diode circuits, which take input data encoded as currents and process it analogously to a feedforward neural network, may yield promising outcomes. Pursuing this research direction could lead to cost-effective AI systems with improved computational efficiency, bridging the gap between quantum-inspired NC systems and practical ML implementations.

REFERENCES

- [1] D. Marković, A. Mizrahi, D. Querlioz, and J. Grollier, “Physics for neuromorphic computing,” *Nat. Rev. Phys.*, vol. 2, no. 9, pp. 499–510,

- 2020.
- [2] M. Nakajima, K. Inoue, K. Tanaka, Y. Kuniyoshi, T. Hashimoto, and K. Nakajima, "Physical deep learning with biologically inspired training method: gradient-free approach for physical hardware," *Nat. Commun.*, vol. 13, p. 7847, 2022.
 - [3] S. Haykin, *Neural Networks: A Comprehensive Foundation*. Pearson-Prentice Hall, Singapore, 1998.
 - [4] I. Goodfellow, Y. Bengio, and A. Courville, *Deep Learning*. MIT Press, 2016.
 - [5] G. Cybenko, "Approximation by superpositions of a sigmoidal function," *Math. Control Signals Syst.*, vol. 2, no. 4, pp. 303–314, 1989.
 - [6] B. Xu, N. Wang, T. Chen, and M. Li, "Empirical evaluation of rectified activations in convolutional network," 2015. [Online]. Available: <https://arxiv.org/abs/1505.00853>
 - [7] P. Ramachandran, B. Zoph, and Q. V. Le, "Searching for activation functions," 2017. [Online]. Available: <https://arxiv.org/abs/1710.05941>
 - [8] I. S. Maksymov, "Analogue and physical reservoir computing using water waves: Applications in power engineering and beyond," *Energies*, vol. 16, p. 5366, 2023.
 - [9] A. H. Abbas, H. Abdel-Ghani, and I. S. Maksymov, "Classical and quantum physical reservoir computing for onboard artificial intelligence systems: A perspective," *Dynamics*, vol. 4, no. 3, pp. 643–670, 2024.
 - [10] D. Marković and J. Grollier, "Quantum neuromorphic computing," *Appl. Phys. Lett.*, vol. 117, no. 15, p. 150501, 2020.
 - [11] J. Dudas, B. Carles, E. Plouet, F. A. Mizrahi, J. Grollier, and D. Marković, "Quantum reservoir computing implementation on coherently coupled quantum oscillators," *NPJ Quantum Inf.*, vol. 9, p. 64, 2023.
 - [12] A. H. Abbas and I. S. Maksymov, "Reservoir computing using measurement-controlled quantum dynamics," *Electronics*, vol. 13, p. 1164, 2024.
 - [13] A. Adamatzky, *Advances in Unconventional Computing. Volume 2: Prototypes, Models and Algorithms*. Springer, Berlin, 2017.
 - [14] G. E. Karniadakis, I. G. Kevrekidis, L. Lu, P. Perdikaris, S. Wang, and L. Yang, "Physics-informed machine learning," *Nat. Rev. Phys.*, vol. 3, pp. 422–440, 2021.
 - [15] D. Peral-García, J. Cruz-Benito, and F. J. García-Peñalvo, "Systematic literature review: Quantum machine learning and its applications," *Comput. Sci. Rev.*, vol. 51, p. 100619, 2024.
 - [16] S. Choi, Y. Salamin, C. Roques-Carnes, R. Dangovski, D. Luo, Z. Chen, M. Horodyski, J. Sloan, S. Z. Uddin, and M. Soljačić, "Photonic probabilistic machine learning using quantum vacuum noise," *Nat. Commun.*, vol. 15, p. 7760, 2024.
 - [17] R. Horodecki, P. Horodecki, M. Horodecki, and K. Horodecki, "Quantum entanglement," *Rev. Mod. Phys.*, vol. 81, no. 2, pp. 865–942, 2009.
 - [18] E. Chitambar and G. Gour, "Quantum resource theories," *Rev. Mod. Phys.*, vol. 91, p. 025001, 2019.
 - [19] M. Lukoševičius and H. Jaeger, "Reservoir computing approaches to recurrent neural network training," *Comput. Sci. Rev.*, vol. 3, pp. 127–149, 2009.
 - [20] G. Tanaka, T. Yamane, J. B. Héroux, R. Nakane, N. Kanazawa, S. Takeda, H. Numata, D. Nakano, and A. Hirose, "Recent advances in physical reservoir computing: A review," *Neural Newt.*, vol. 115, pp. 100–123, 2019.
 - [21] K. Nakajima, "Physical reservoir computing—an introductory perspective," *Jpn. J. Appl. Phys.*, vol. 59, p. 060501, 2020.
 - [22] R. M. Kent, W. A. S. Barbosa, and D. J. Gauthier, "Controlling chaos using edge computing hardware," *Nat. Commun.*, vol. 15, p. 3886, 2024.
 - [23] L. Esaki, "New phenomenon in narrow germanium $p - n$ junctions," *Phys. Rev.*, vol. 109, pp. 603–604, 1958.
 - [24] L. L. Chang, L. Esaki, and R. Tsu, "Resonant tunneling in semiconductor double barriers," *Appl. Phys. Lett.*, vol. 12, pp. 593–595, 1974.
 - [25] Y. Yilmaz and P. Mazumder, "Image processing by a programmable grid comprising quantum dots and memristors," *IEEE Trans. Nanotechnol.*, vol. 12, no. 6, pp. 879–887, 2013.
 - [26] Y. Feng, M. Tang, Z. Sun, Y. Qi, X. Zhan, J. Liu, J. Zhang, J. Wu, and J. Chen, "Fully flash-based reservoir computing network with low power and rich states," *IEEE Trans. Electron Devices*, vol. 70, no. 9, pp. 4972–4975, 2023.
 - [27] A. G. Revesz and P. L. Fleming, "Tunnel diodes in satellite communications," *COMSAT Tech. Rev.*, vol. 8, pp. 257–274, 1978.
 - [28] G. Binnig and H. Rohrer, "Scanning tunneling microscopy—from birth to adolescence," *Rev. Mod. Phys.*, vol. 59, pp. 615–625, Jul 1987.
 - [29] S. Abel, N. Chancellor, and M. Spannowsky, "Quantum computing for quantum tunneling," *Phys. Rev. D*, vol. 103, no. 1, p. 016008, 2021.
 - [30] Z. Chen, Z. Xiao, M. Akl, J. Leugring, O. Olajide, A. Malik, N. Dennler, C. Harper, S. Bose, H. A. Gonzalez, J. Eshraghian, R. Pignari, G. Urgese, A. G. Andreou, S. Shankar, C. Mayr, G. Cauwenberghs, and S. Chakrabarty, "On-off neuromorphic ISING machines using Fowler-Nordheim annealers," 2024. [Online]. Available: <https://arxiv.org/abs/2406.05224>
 - [31] D. D. Georgiev and J. F. Glazebrook, "Quantum tunneling of Davydov solitons through massive barriers," *Chaos Soliton. Fract.*, vol. 123, pp. 275–293, 2019.
 - [32] I. S. Maksymov, "Quantum-tunneling deep neural network for optical illusion recognition," *APL Mach. Learn.*, vol. 2, no. 3, p. 036107, 2024.
 - [33] A. H. Abbas, H. Abdel-Ghani, and I. S. Maksymov, "Edge-of-chaos and chaotic dynamics in resistor-inductor-diode-based reservoir computing," *IEEE Access*, vol. 13, pp. 18 191–18 199, 2025.
 - [34] A. Messiah, *Quantum Mechanics*. North-Holland Publishing Company, Amsterdam, 1962.
 - [35] S. Sze and K. K. Ng, *Physics of Semiconductor Devices*, 3rd ed. Hoboken, NJ: John Wiley & Sons, 2006.
 - [36] M. Lukoševičius, "A practical guide to applying echo state networks," in *Neural Networks: Tricks of the Trade, Reloaded*, G. Montavon, G. B. Orr, and K.-R. Müller, Eds. Berlin: Springer, 2012, pp. 659–686.
 - [37] I. Ortega-Piwonka, O. Piro, J. Figueiredo, B. Romeira, and J. Javaloyes, "Bursting and excitability in neuromorphic resonant tunneling diodes," *Phys. Rev. Appl.*, vol. 15, p. 034017, Mar 2021.
 - [38] J. Schulman, H. De Los Santos, and D. Chow, "Physics-based rtd current-voltage equation," *IEEE Electron Device Letters*, vol. 17, no. 5, pp. 220–222, 1996.
 - [39] I. S. Maksymov and A. D. Greentree, "Coupling light and sound: giant nonlinearities from oscillating bubbles and droplets," *Nanophotonics*, vol. 8, no. 3, pp. 367–390, 2019.
 - [40] D. J. Gauthier, E. Bollt, A. Griffith, and W. A. S. Barbosa, "Next generation reservoir computing," *Nat. Commun.*, vol. 12, p. 5564, 2021.
 - [41] I. S. Maksymov, "Physical reservoir computing enabled by solitary waves and biologically inspired nonlinear transformation of input data," *Dynamics*, vol. 4, no. 1, pp. 119–134, 2024.
 - [42] S. Murat H., "A brief review of feed-forward neural networks," *Communications Faculty of Sciences University of Ankara Series A2-A3 Physical Sciences and Engineering*, vol. 50, no. 1, p. 11–17, 2006.
 - [43] A. L. Caterini and D. E. Chang, *Deep Neural Networks in a Mathematical Framework*, 1st ed. Springer Publishing Company, Incorporated, 2018.
 - [44] B. M. N. Smets, "Mathematics of neural networks (lecture notes graduate course)," 2024. [Online]. Available: <https://arxiv.org/abs/2403.04807>
 - [45] K. Hornik, M. Stinchcombe, and H. White, "Multilayer feedforward networks are universal approximators," *Neural Netw.*, vol. 2, no. 5, pp. 359–366, 1989.
 - [46] M. Maksimovic and I. S. Maksymov, "Quantum-cognitive neural networks: Assessing confidence and uncertainty with human decision-making simulations," *Big Data Cogn. Comput.*, vol. 9, no. 1, 2025. [Online]. Available: <https://doi.org/10.3390/bdcc9010012>
 - [47] G. Keren, S. Sabato, and B. Schuller, "Analysis of loss functions for fast single-class classification," *Knowl. Inf. Syst.*, vol. 62, no. 1, pp. 337–358, 2020.
 - [48] L. Deng, "The mnist database of handwritten digit images for machine learning research [best of the web]," *IEEE Signal Processing Magazine*, vol. 29, no. 6, pp. 141–142, 2012.
 - [49] J. McNaughton, "Tunnel diode activation functions," <https://github.com/jakemcnaughton/TunnelDiodeActivationFunction>, 2025.
 - [50] A. Baldominos, Y. Saez, and P. Isasi, "A survey of handwritten character recognition with MNIST and EMNIST," *Appl. Sci.*, vol. 9, no. 15, 2019.
 - [51] K. M. Bastiaans, T. Benschop, D. Chatzopoulos, D. Cho, Q. Dong, Y. Jin, and M. P. Allan, "Amplifier for scanning tunneling microscopy at MHz frequencies," *Rev. Sci. Instrum.*, vol. 89, no. 9, p. 093709, 2018.
 - [52] B. Ulmann, *Analog and Hybrid Computer Programming*. De Gruyter Oldenbourg, 2020.
 - [53] Y. Lv, Y. Wang, T. Meng, Q. Wang, and W. Chu, "Review on thermal management technologies for electronics in spacecraft environment," *Energy Storage Sav.*, vol. 3, no. 3, 2024.
 - [54] NASA, "Thermal control for small spacecraft," <https://www.nasa.gov/smallsat-institute/sst-soa/thermal-control/>, 2025, [accessed 2025 Feb 10].